Paper III

C. Sætre, C. A. Barth, J. Stadsnes, N. Østgaard, S. M. Bailey, D. N. Baker, G. A. Germany, and J. W. Gjerloev (2006)

Thermospheric nitric oxide at higher latitudes - Model calculations with auroral energy input

Submitted to *Journal of Geophysical Research*

Thermospheric nitric oxide at higher latitudes - Model calculations with auroral energy input

C. Sætre[1], C. A. Barth[2], J. Stadsnes[1], N. Østgaard[1], S. M. Bailey[3], D. N. Baker[2], G. A. Germany[4], and J. W. Gjerloev[5]

Abstract. The nitric oxide (NO) density in the lower thermosphere has been calculated by a photochemical model for NOx and compared with measured NO densities. At higher latitudes the most important contributor for NO density increases is energetic electron precipitation. The electron energy input is divided in geographic areas of 5° latitude and 24° longitude for a continuous time interval of four days. The energy is derived in two ways; from auroral ultraviolet (UV) and X-ray measurements, and estimated from ground magnetometer measurements. These are used as input for the photochemical NOx model. The UV and X-ray measurements are from the Ultraviolet Imager (UVI) and the Polar Ionospheric X-ray Imaging Experiment (PIXIE), both onboard the Polar spacecraft. For the time intervals without UVI and PIXIE measurements, a parametrization of the electron energy flux from ground magnetic measurements were used. This parametrization was based on data from the SuperMAG database compared to UVI/PIXIE derived electron energy fluxes. The perturbation in the southward ground magnetic component is found to be linearly related to the precipitating electron energy flux derived from UVI and PIXIE measurements. The event is from 30 April (day 120) until 4 May 1998, where the onset of a geomagnetic storm occurred 2 May (day 122). The modeled NO density is compared with NO measurements from the Student Nitric Oxide Explorer (SNOE). The results show an overall larger modeled nitric oxide density at auroral latitudes than what was measured by SNOE. The largest discrepancies were for the day of the storm onset, when the background atmosphere was distorted by Joule heating. The next day, when the atmosphere had settled down, the agreement between the model and the observations was far better.

1. Introduction

Nitric oxide in the upper atmosphere is a minor constituent which has important properties for the radiative cooling and for the chemical composition. The lifetime of NO at these altitudes is about one day for sunlit conditions, and NO can hence function as a trace element for atmospheric motion. There are also predictions and observations that thermospheric NO can be transported to lower altitudes within a strong winter polar vortex to the stratosphere, where NO can react with ozone [e.g. *Solomon et al.*, 1982; *Randall et al.*, 2005, 2006]. Precipitating energetic particles cause dissociation, ionization and excitation of the upper atmospheric molecules and atoms. The excited nitrogen atoms will react with molecular oxygen and give production of NO. The maximum density of NO is in the lower thermosphere, around 110 km altitude. NO is mainly destroyed by photodissociation from solar far ultraviolet radiation, and the subsequent reaction with ground state nitrogen. The NO density in the lower thermosphere varies with the time of day, the solar radiation, and the auroral particle precipitation. Photoelectrons produced from solar soft X-rays and extreme ultraviolet (EUV), cause NO increase at all latitudes where there is sunlight. At higher latitudes auroral electron precipitation dominates the NO production. The increase in NO from auroral electron energy input has been of interest for several decades. Models have been established for calculating the NO density in the lower thermosphere. However, the changes of NO at the auroral latitudes are still not fully accounted for by the models, especially considering the heating effects on the background atmosphere, and transport by neutral winds.

Siskind et al. [1989b] investigated the variation of thermospheric nitric oxide during an auroral storm at low and middle latitudes, where the effect of enhanced particle and Joule heating and solar soft X-rays were dominant for the NO density. The companion paper *Siskind et al.* [1989a], analyzed the response of NO at higher latitudes during an auroral storm. NO density measurements showed a factor of 3 increase from one day prior to the storm to one day after the storm. To calculate this response they used a time dependent photochemical NOx model based on the work of *Cleary* [1986]. The history of the particle precipitation with

[1]Department of Physics and Technology, University of Bergen, Norway.
[2]Laboratory for Atmospheric and Space Physics, University of Colorado, Boulder, Colorado, USA.
[3]Geophysical Institute, University of Alaska, Fairbanks, Alaska, USA.
[4]Center for Space Plasma and Aeronomic Research, University of Alabama in Huntsville, Huntsville, Alabama, USA
[5]Applied Physics Laboratory, Johns Hopkins University, Laurel, Maryland, USA.

Paper number .
0148-0227/06/$09.00

characteristic energy and energy flux for specific geographical location, was used as input to the model. This was derived from an empirical model of global precipitation patterns constructed from the TIROS/NOAA auroral particle observations [*Foster et al.*, 1986; *Fuller-Rowell and Evans*, 1987]. The particle precipitation was ordered by an activity parameter, the hemispheric particle power input (HPI), estimated from observations by NOAA 6 and 7. The calculated lower thermosphere NO density was compared to the NO density measured by the Solar Mesospheric Explorer (SME). The model overestimated the NO density at all altitudes both for the quiet day before the storm, and for the day after the storm. The discrepancy could be due to a too large yield of excited atomic nitrogen (60-75%) produced from energetic electron impact on molecular nitrogen. Vertical winds in the auroral arc could also be important in damping the NO response to increased particle precipitation. Neutral wind transport of NO were not accounted for in the model. It was also emphasized that a more accurate time history of the particle precipitation, than that derived from an empirical model, would be required.

Another version of this photochemical model for calculating the NO density was developed by *Barth* [1992], and improved further by *Bailey et al.* [2002]. Previously the model has been run with solar soft X-ray measurements from SNOE as input for photoelectrons, for estimation of NO density at lower latitudes [*Barth and Bailey*, 2004]. Comparisons with NO measured from SNOE showed a remarkable agreement at latitudes below 30° north and south. The photochemical model can also be used for deriving the total electron energy deposition from NO measurements by SNOE. *Sætre et al.* [2006] compared this energy deposition from thermospheric NO densities, with that derived from time-integrated X-ray bremsstrahlung measurements from PIXIE. This study found that at higher latitudes the NOx photochemical model underestimated the energy deposition compared to the PIXIE measurements.

In the present work we calculate the NO density at higher latitudes by the use of this photochemical model, with both photoelectron and auroral electron energy input. The auroral energy flux and characteristic energy are derived not only from PIXIE measurements as in *Sætre et al.* [2006], but from UVI and PIXIE measurements, to estimate the electron energies from 1 keV to 100 keV. UVI and PIXIE had a global view of the northern auroral oval for ∼10 consecutive hours of each ∼18 hour orbit. Since the NO gas has a lifetime of ∼1 day in sunlight, the auroral energy input for the NOx model needs to be continuous throughout an event. For the time intervals without UVI and PIXIE measurements, we use a parametrization of the electron energy flux based on ground magnetometer measurements.

The comparisons between the nitric oxide density calculated by the photochemical model including auroral energy input, and the density measured by SNOE, show that the model generally overestimates the amount of NO at higher latitudes. The measured nitric oxide profiles indicate that the response of the lower thermospheric nitric oxide to the energetic electron precipitation, was suppressed the day of the storm onset. The source for this damping, is not included in the model calculations. For the day after the storm onset, when the background atmosphere was more stable again, the modeled nitric oxide density is in better agreement with the observations.

2. Instruments and methods

2.1. SNOE NO observations

The Student Nitric Oxide Explorer (SNOE) measured the NO column density in the lower thermosphere. The satellite had a sun-synchronous orbit at 556 km altitude, with the ascending node at 10:30 SLT. The measurement technique was limb spectral observations of the fluorescence of NO molecules by solar radiation. Hence, the measurements were done on the dayside of the SNOE orbit only. The column emission rate from the NO (0,1) gamma band at 237 nm, is related to the NO column density by the photon scattering coefficient, called the g-factor [*Barth et al.*, 2004]. The g-factor is the possibilities for absorption of sunlight at a wavelength by an atmospheric molecule, and the subsequent fluorescent emission.

In this study the NO density has been arranged in 5° latitude and 24° longitude boxes. The spatial resolution of the SNOE NO measurements were 5° latitude, 3.3 km altitude, and 33 km in the zonal direction.

2.2. NOx model

The model for nitric oxide chemistry used in this study is a new version of a photochemical model [*Cleary*, 1986; *Siskind et al.*, 1989b, a, 1990, 1995; *Barth*, 1992], with updated reaction rate coefficients and excitation ratios from *Barth et al.* [1999]; *Bailey et al.* [2002]. For example, the yield of $N(^2D)$ from dissociation of N_2 by energetic electrons, is reduced to 0.54 [*Zipf et al.*, 1980]. The model is time-dependent and one-dimensional. It includes vertical transport of $N(^4S)$ and NO by eddy and molecular diffusion. The electron transport is calculated using the *glow* model of *Solomon et al.* [1988]; *Solomon and Abreu* [1989], which includes the energetic electron transport [*Banks and Nagy*, 1970] for both photoelectrons and auroral electrons. The NOx model uses photochemical equilibrium to calculate the vertical profiles of NO, $N(^4S)$, $N(^2D)$, NO^+, O_2^+, N_2^+, O^+ and $O^+(^2D)$. The extreme ultraviolet solar flux (20-103 nm) is calculated from the model of *Hinteregger et al.* [1981], with the 10.7 nm solar radio flux as input parameter. The solar soft X-ray irradiance used in the NOx model was measured by SNOE [*Bailey et al.*, 2000]. The photoelectron fluxes used in the model are found to correspond well with measured fluxes [*Solomon et al.*, 2001]. Modeled nitric oxide densities at lower latitudes produced from energetic photoelectrons, are found to be in good agreement with measured densities [*Barth and Bailey*, 2004]. The model for the background neutral atmosphere is the NRLMSISE-00 model [*Picone et al.*, 2002], where daily values of the 10.7 nm solar flux and the 3 hour Ap geomagnetic index are used as inputs. The MSIS models are based on a hydrostatic model of *Bates* [1959].

The N_2 ionization rate responds directly to the electron energy input. The NO density increase is an accumulated response of the increased ionization and dissociation. The amount of NO also varies throughout the day as a function of insolation. However, this effect is minimal compared to the response of the auroral energy input at higher latitudes.

The NOx model includes chemical and diffusion loss processes of NO. Some of these processes transform NO into other odd nitrogen species. Photodissociation of NO and the following $N(^4S)$ reaction with another NO molecule, have the end product N_2 and O. The effective lifetime of this process is 19.6 hours [*Minschwaner and Siskind*, 1993].

2.3. Electron precipitation - UVI and PIXIE auroral observations

The Ultraviolet Imager (UVI) [*Torr et al.*, 1995] and the Polar Ionospheric X-ray Imaging Experiment (PIXIE) [*Imhof et al.*, 1995] on board the Polar spacecraft, measured the auroral signatures of precipitating electrons of ultraviolet emissions and X-ray bremsstrahlung. These measurements provide a global map of the precipitating electrons.

PIXIE was a pinhole camera observing the X-ray bremsstrahlung in the energy range ~3-22 keV. The spatial resolution was ~700 km above the northern hemisphere, where Polar had it's apogee in 1998. The data processing of the PIXIE measurements is described in *Østgaard et al.* [1999], and the method for deriving a four parameter electron energy spectrum from the PIXIE data is described in *Østgaard et al.* [2000, 2001].

UVI observes ultraviolet emissions in the Lyman-Birge-Hopfield (LBH) band. These measurements are separated in the LBH-short and LBH-long bands. LBH-long emissions are proportional to the precipitating electron energy flux. The difference in absorption by molecular oxygen of the two LBH bands provides information on the average energy of the precipitating electrons. Due to the wobbling of the pointable pedestal on the Polar satellite, the spatial resolution of UVI from apogee is degraded from the nominal value of 35 km to approximately ten times that value in the direction of the wobble. The spatial resolution perpendicular to the wobble direction is unaffected. The method for deriving a two parameter electron energy spectrum from the UVI measurements is described in *Germany et al.* [1997, 1998a, b].

The method of deriving the electron energy spectrum from these two different observation techniques is described in *Østgaard et al.* [2001], where the result also has been compared with electron energy spectra from DMSP low-altitude satellite measurements. The combined UVI and PIXIE measurements provide electron energy spectra for the electron energy range 1-100 keV. Electrons with mean energy around 5 keV, deposit most of their energy in the altitude region important for NO production (between 100 and 110 km altitude).

For this work we used the electron energy spectra as input in the photochemical NOx model. The spectra for 10 minute intervals derived from UVI and PIXIE measurements, were two parameter Maxwell spectra. The electron energy flux and mean energy were then averaged for every one hour intervals. Thus the hourly energy parameters put into the NOx model were averaged Maxwellian fits to 6 combined UVI and PIXIE 10 minute resolution measurements. There were intervals of up to ~10 hours of continuous measurements from UVI and PIXIE for the event studied here.

2.4. Electron precipitation and geomagnetic perturbations

Because of the lack of continuous measurements of the electron precipitation, we aimed for using ground magnetometer observations of the geomagnetic perturbations as a proxy for the auroral electron energy input. The main purpose was to obtain a map of the energy input from electron precipitation, persistent over several days, for input in the NOx photochemical model. The neutral particles are not governed by the magnetic and electric fields. They corotate with the Earth. Hence, the coordinate system used in this comparison was geographical.

The geomagnetic disturbances in the north (MAG) magnetic component (ΔN) at higher latitudes, are connected to ionospheric currents known as the electrojets. The westward electrojet, giving a negative deflection in ΔN, is related to the Hall conductance, which again is connected to the energetic electron precipitation [e.g. *Baumjohann and Kamide*, 1984; *Ahn et al.*, 1999; *Gjerloev and Hoffmann*, 2001; *Østgaard et al.*, 2002]. The eastward electrojet is thought to be more strongly governed by the electric field [*Baumjohann and Kamide*, 1984; *Ahn et al.*, 1999; *Gjerloev and Hoffmann*, 2001]. Thus for this work we correlate the maximum negative perturbation of the local north magnetic component, ΔN<0, from the ground based measurements, with the precipitating electron flux derived from UVI and PIXIE observations. Previous studies of geomagnetic indices and their connections to electron precipitation, have mainly been focused on the global AE indices [e.g. *Gjerloev and Hoffmann*, 2001; *Østgaard et al.*, 2002]. Here we apply ground magnetometer data from the SuperMAG database, which consists of more than 100 stations located at higher northern latitudes. The comparisons between ΔN and precipitating electron flux, were made within longitude sectors of 24°.

A two parameter Maxwell electron energy spectrum is derived from UVI and PIXIE measurements for consecutive 10 minute intervals. Then the hourly mean of the electron energy flux averaged over a 20° latitude band (50°-70°N) around the auroral oval, is compared to the hourly mean of the ΔN<0 values for the concurrent longitudinal sector. As mentioned above, the ΔN ground perturbations are connected to the Hall conductivity, which again is related to the electron precipitation. The electron energies contributing to the Hall conductance are above ~ 3keV. The electron energy

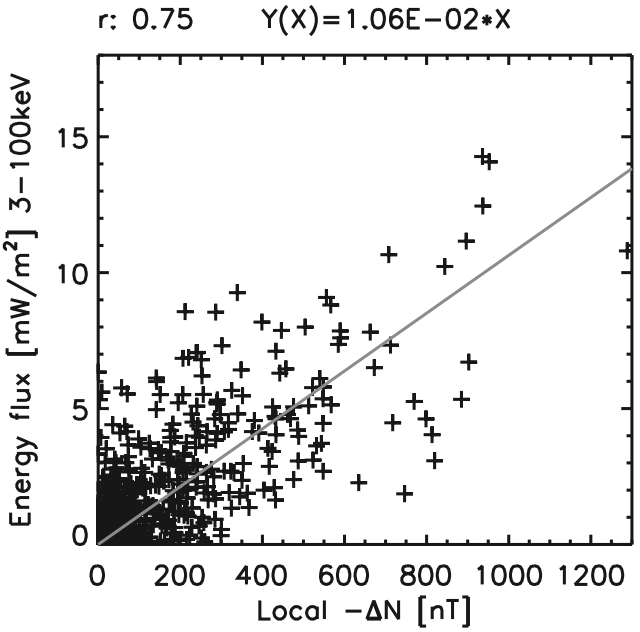

Figure 1. Precipitating electron (3-100 keV) energy flux averaged over a 20° auroral latitude band, plotted against the maximum negative perturbation of the ground geomagnetic north component, ΔN<0. The values are hourly means, within 24° geographic longitude sectors, for days 120, 122, 123, and 177 of 1998. There are 589 points in total, most of them at low values. The correlation coefficient is 0.75. The linear fit has a slope of 0.0106 [mW m^{-2} nT^{-1}].

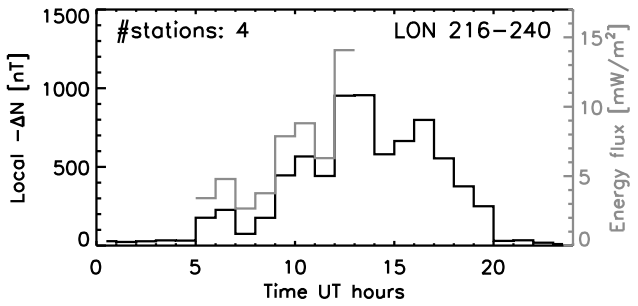

Figure 2. Hourly mean of the negative ground north geomagnetic perturbation, $\Delta N<0$ (black, units of nT). Electron energy flux (3-100 keV) derived from UVI and PIXIE observations, hourly mean averaged over 20° auroral latitude band (gray, units of mW m^{-2}). Both data sets are within geographic longitude sector 216°-240°E, day 122 of 1998, and are plotted as functions of universal time. The number of stations used to get the $\Delta N<0$ values within this 24° longitude sector is indicated in the upper left corner.

flux used in these comparisons is just for the energy range 3-100 keV, the electron energies assumed to give changes in the $\Delta N<0$ ground geomagnetic field.

The global magnetometer network, SuperMAG, is a data set provided by more than 200 ground magnetometer stations [*Gjerloev et al.*, 2004]. This network gives good global coverage and continuous measurements of the ground geomagnetic perturbations. The magnetometer data has a common baseline removal technique, the same time resolution and the same coordinate system. In the present study, only the stations for the northern hemisphere are used, in all more than 100 stations. However, there are areas like Siberia where there might only be one or two stations available within a 24° longitude sector. The ΔN perturbations in these sectors were for the four events investigated here, more often showing high values when high auroral activity than no deflection. Thus we chose to include all longitude sectors in our comparisons. The stations are mainly conveniently located in close proximity to the auroral oval. In the sectors where the number of stations are few, the stations also have relatively good longitudinal coverage.

The comparisons for all the four days, for all sectors, and all hours of UVI and PIXIE measurements, are gathered in one scatter plot, figure 1. The correlation of the data sets is 0.75. We assume there is overall no essential electron precipitation when $\Delta N=0$. The cluster of low-value points is not so that a linear fit would cross the y-axis below zero. Hence, we have calculated a linear fit of the comparisons through origin, using the least square method.

The comparisons were done for all hours where UVI and PIXIE were measuring, also for times and areas with low activity. Areas outside the UVI and PIXIE's field of views were of course not included. To understand more of the details behind the spreading of the data points in figure 1, we have plotted the hourly means of the periods with $\Delta N<0$ and the electron energy flux as functions of universal time. Figure 2 is an example of a well correlated high activity event, 216°-240°E, day 122 of 1998. The black histogram is the hourly mean $\Delta N<0$ for the region, and the grey histogram is the hourly mean electron energy flux derived from UVI/PIXIE. The maximum activity was 2 hours after midnight for this sector. Overall, the night sector shows a fairly good correlation between the two data sets. Sometimes, though, the electron energy flux implies a quite larger activity than the ground magnetometer data. Such an example is shown in figure 3. There are 14 geomagnetic stations for this sector, so one would assume that this was sufficient for registering any ionospheric current above the region. 11 of the stations are, however, part of the magnetometer array at the west coast of Greenland. If the currents related to the auroral activity were located quite south of these stations, a much fainter deflection would be registered. A situation where the geomagnetic $\Delta N<0$ perturbations gave relatively larger values than the electron energy flux derived from UVI and PIXIE, is displayed in figure 4, from local time ~4 (corresponding to 10 UT in the figure) and onward. The field of views for UVI and PIXIE were quite good for this longitude sector and time interval. The first five hours of the event, where the actual longitude interval was in the local midnight to early morning sector, the correlation was exceptionally good. On the nightside the ionospheric current systems are believed to be controlled by the Hall conductance [e.g. *Kamide and Vickrey*, 1983; *Sugino et al.*, 2002; *Gjerloev and Hoffmann*, 2001]. In the morning sector, however, the currents can be more influenced by the electric field [*Kamide and Kokubun*, 1996; *Gjerloev and Hoffmann*, 2001]. Thus the relative larger amplitudes of the $\Delta N<0$ perturbations in the later part of the morning sector, were probably caused by an increased convectional electric field, and were not directly related to the electron precipitation through increased Hall conductance.

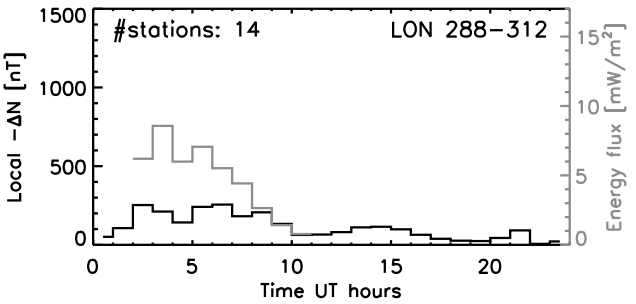

Figure 3. Same type of plot as figure 2, for 288°-312°E, day 177 of 1998.

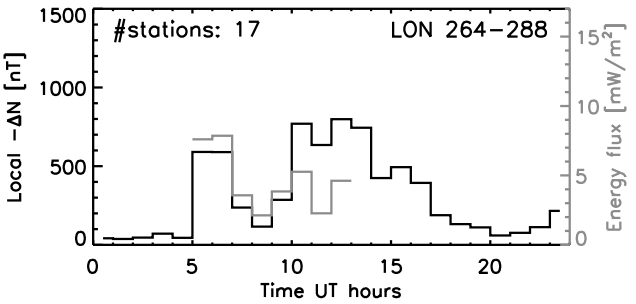

Figure 4. Same type of plot as figure 2, for 264°-288°E, day 122 of 1998.

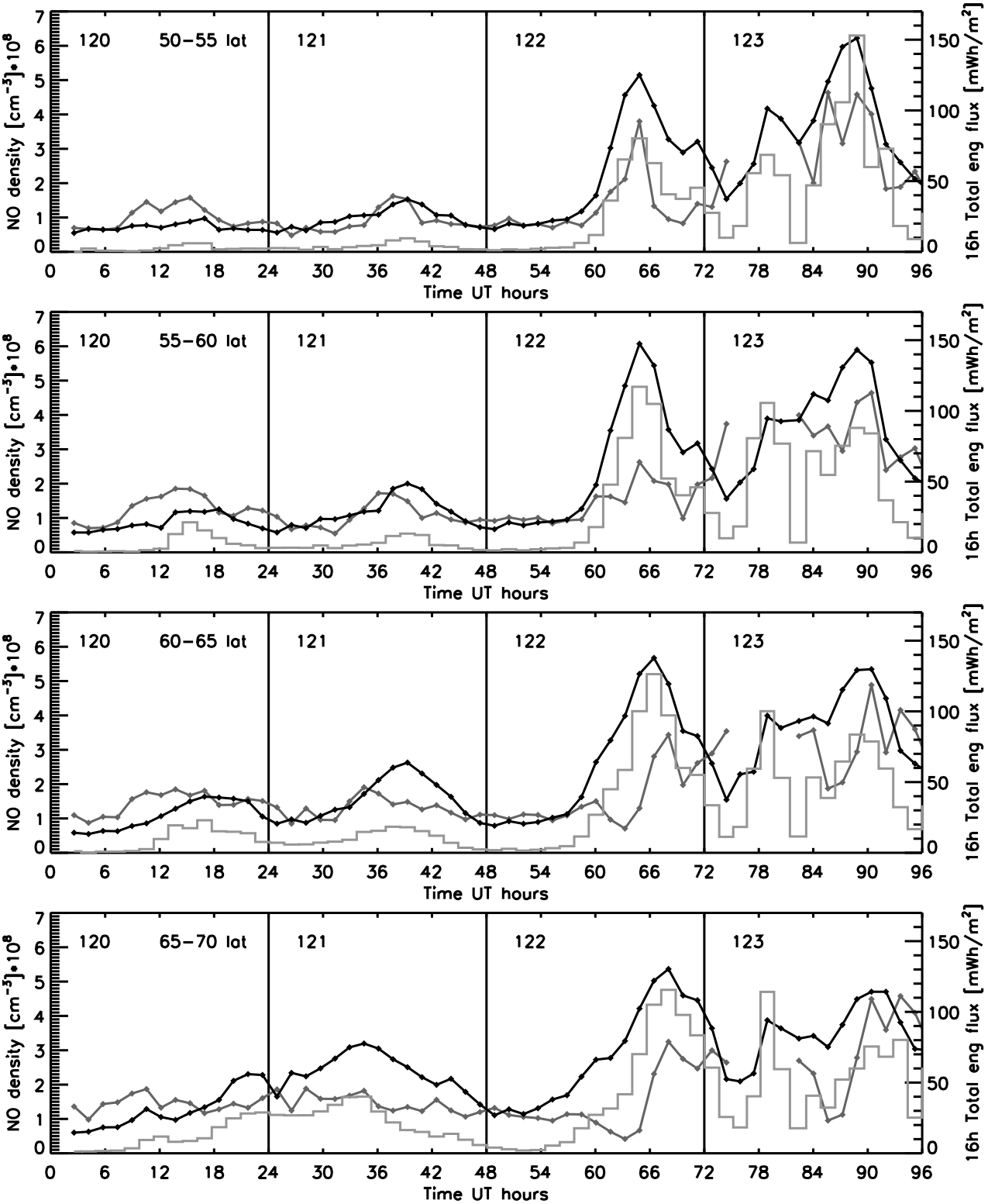

Figure 5. Nitric oxide density [molecules/cm^3] at 110 km altitude as function of universal time for the days 120 to 123 of 1998. The black curve is the modeled NO density, and the gray curve is the NO density measured by SNOE. The light gray histogram displays the total electron energy flux [mWh/m^2] the preceding night and morning (16 hours) for each of the longitude sectors of the SNOE dayside measurements. Each of the days, SNOE orbit number 1 between 120° and 144°E, occurred at ~00:30 UT. The satellite passes then moved westward. The orbit number 6 for longitudes 336°-360°E, was at ~10:30 UT. And finally, orbit number 15, 144°-168°E, occurred at ~23:00 UT. The steps between each orbit was 24° longitude, in the westward direction.

To summarize, the comparisons between hourly mean of $\Delta N<0$ perturbations from ground magnetometer data, and energetic electron energy flux from UVI and PIXIE observations for geographical longitude sectors, gave a correlation of 0.75. We find this result significant, and conclude that ground $\Delta N<0$ perturbations may be used together with UVI and PIXIE data to provide geographical maps of the energetic electron precipitation which are continuous in time. The fluctuations around the linear parametrization are believed to be more or less levelled out when model calculations are done for several consecutive hours (~8 hours and more).

3. Results NOx model

The NOx model calculated the nitric oxide density in 24° longitude times 5° latitude boxes. The input parameters were the average auroral electron energy flux and characteristic energy, for the same geographical areas, in one hour intervals. The modeled NO density was compared to that measured by SNOE. The comparisons were done as functions of universal time, latitude, altitude, and solar local time for specific longitude intervals for each SNOE orbit.

In figure 5 the NO density from the model (black curve) and the NO density from SNOE measurements (gray curve with dots), at 110 km altitude, are plotted as functions of universal time from day 120 until day 124 of 1998. The four latitude sectors between 50°N and 70°N are displayed. The time resolution for this plot is ~1.5 hours (distance between the dots), which is the time between the SNOE orbits. The location in longitude varies with 24 degrees for each of these time steps. Thus the plot gives the overall variations in nitric oxide in the lower thermosphere during the course of the geomagnetic storm. Also shown is the total auroral electron energy flux for the preceding 16 hours (from 18 SLT the previous day to 10 SLT) for the particular regions compared (gray histogram). The energy fluxes are derived directly from UVI/PIXIE measurements, and for the hours when UVI/PIXIE did not cover the northern auroral oval, from the magnetic perturbation parametrization. Each column of the energy flux histogram consists of the sum of auroral activity for the particular longitude region for the evening, night, and morning hours before the SNOE measurements for the region.

The first day of comparisons, 120, the model has not had time to respond to the energy input and we focus on the comparisons for the next three days, 121, 122 and 123 of 1998. On day 121 the geomagnetic activity was low. There was, however, some electron precipitation at latitude bands 50-55 N and 55-60 N that produced a small increase in the observed nitric oxide density. The NOx model calculation matched this increase very nicely. There was additional electron precipitation at latitude bands 60-65 N and 65-70 N that caused the

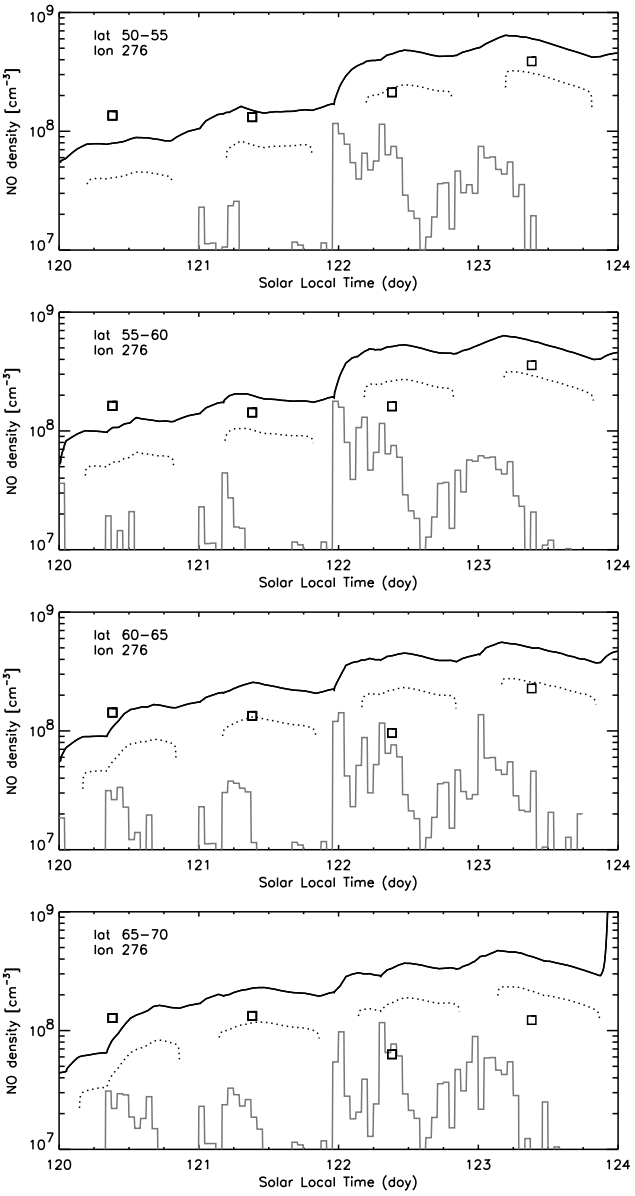

Figure 6. Solar local time variations of the NOx model calculations at 106 km altitude for the days 120 to 123 of 1998, four latitude sectors around 276° east. The solid black line is the NO density calculated from the NOx model. The squares are the NO density measured by SNOE for the particular region. The dotted line is the NO photodissociation rate, and the gray histogram displays the N_2 auroral ionization rate. The scales for these two parameters are chosen arbitrarily.

NOx model to predict an increase in nitric oxide density that was not reflected in the NO measurements from SNOE.

The next day, 122, where the onset of the geomagnetic storm occurred ~05:30 UT, there was a rather good correspondence between the two density profiles prior to the storm. From ~12 to 15 UT for the three most northerly sectors, there was a decrease in the measured NO density, while there was a profound activity

measured by UVI and PIXIE for these regions. After ~15 UT the measured density increased strongly in accordance with the auroral energy input to the model. However, the amplitude of the measured NO density was substantially less than the modeled density. During the last hours of day 122 and the first hours of day 123, the measured NO density was actually enhanced while the modeled NO density decreased. This also occurred the last hours of day 123.

On day 123 there were four orbits during the first half of the day where there were no SNOE measurements. During the second half of the day, the agreement between the model calculations and the observations improved. In latitude bands 60-65 N and 65-70 N, there was a decrease in measured NO density compared to the model result between 13:30 and 15:00 UT. During the following couple of hours the measured density increased showing a good agreement with the observations.

When interpreting these changes in nitric oxide as function of universal time, it is important to remember that the longitude sectors are not the same from one measurement time to another.

Figure 6 shows the NO density variations as function of solar local time for one of the longitude sectors (276°E) that experienced a clear reduction of the measured NO density. This reduction was not expected, since the UVI and PIXIE data clearly showed an input of auroral electron energy for this region, as shown by the relatively high N_2 auroral ionization rate in figure 6. The corresponding universal time for the SNOE measurements for this longitude sector was ~15 UT. This figure gives the modeled NO density at 106 km altitude (black solid curve) as a function of solar local time. Also shown is the measured NO density as squares, one measurement for the specific longitude sector for each day. The nitric oxide photodissociation rate (dotted line) and the N_2 auroral ionization rate (gray histogram) are both plotted on an arbitrary scale. The auroral ionization rate is directly related to the input precipitation electron energy flux from the UVI and PIXIE measurements, and the SuperMAG parametrization. The parametrization was averaged over all the four latitude sectors, and hence the hours where UVI and PIXIE had no observations, the energy flux was the same for all the latitude sectors. For the example given in figure 6, we see that for the two lowest latitudes there was a fairly good agreement between the model and the SNOE data for day 121. The increase in the measured NO density for the next day, 122, was not nearly large enough compared to the modeled NO density. For the two upper latitude sectors the measured NO density at 106 km altitude actually decreased substantially from day 121 to day 122, in spite of the observed auroral activity at these latitudes. For all latitudes there was a clear increase in the measured NO density from day 122 to day 123. However, it seems like the basis on day 122 was too low compared to the modeled density to give a good agreement between the two profiles on day 123 either. Clearly something happened on day 122 that strongly suppressed the effect on nitric oxide from auroral precipitation.

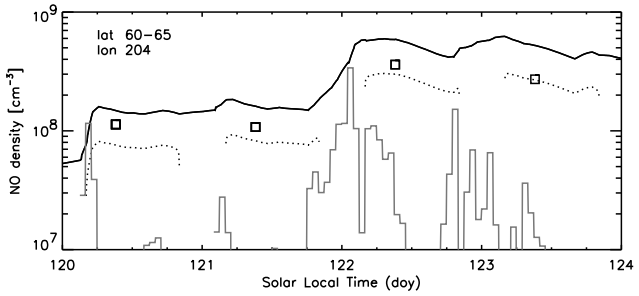

Figure 7. Same type of plot as figure 2, for 204° east and 60-65° north.

Figure 7 gives an example of how the modeled NO density is larger than the measured NO density for all the four days. The factor between the model result and the measured density seems to remain the same throughout the entire period. This case is for 204° E, 60°-65° N, corresponding to ~20 UT for the SNOE measurements. Unlike the example given in figure 6, the SNOE observations show a clear increase of the NO density on day 122 due to the geomagnetic storm.

The altitude profiles of the nitric oxide densities for 228° E for all the four latitude sectors for day 122 (upper) and day 123 (lower) of 1998, are shown in figure 8. The universal time for the SNOE measurements at this longitude was ~18 UT. The modeled nitric oxide density on day 122 was overall larger than that measured by SNOE. This was especially evident at altitudes above ~120 km. The auroral electron energy flux used as input for the model was not particularly large for this longitude sector during either of these days. We see that on day 122, the model displays none of the structures of the measured NO profile above ~120 km altitude. The nitric oxide altitude profiles were better correlated at all altitudes on day 123. A few of the cases with the most evident differences between the model and the measured NO density for day 123 had a much larger difference the day before (day 122).

4. Discussion

The objective for this study was to validate the calculation of lower thermospheric nitric oxide at higher latitudes by a photochemical model [*Barth*, 1992; *Bailey et al.*, 2002]. Previous work with the same model gave good agreement with observed nitric oxide densities at low latitudes where the effect of electron impact on the production of nitric oxide is from photoelectrons which are produced by the action of solar soft X-rays on molecular nitrogen and atomic oxygen.

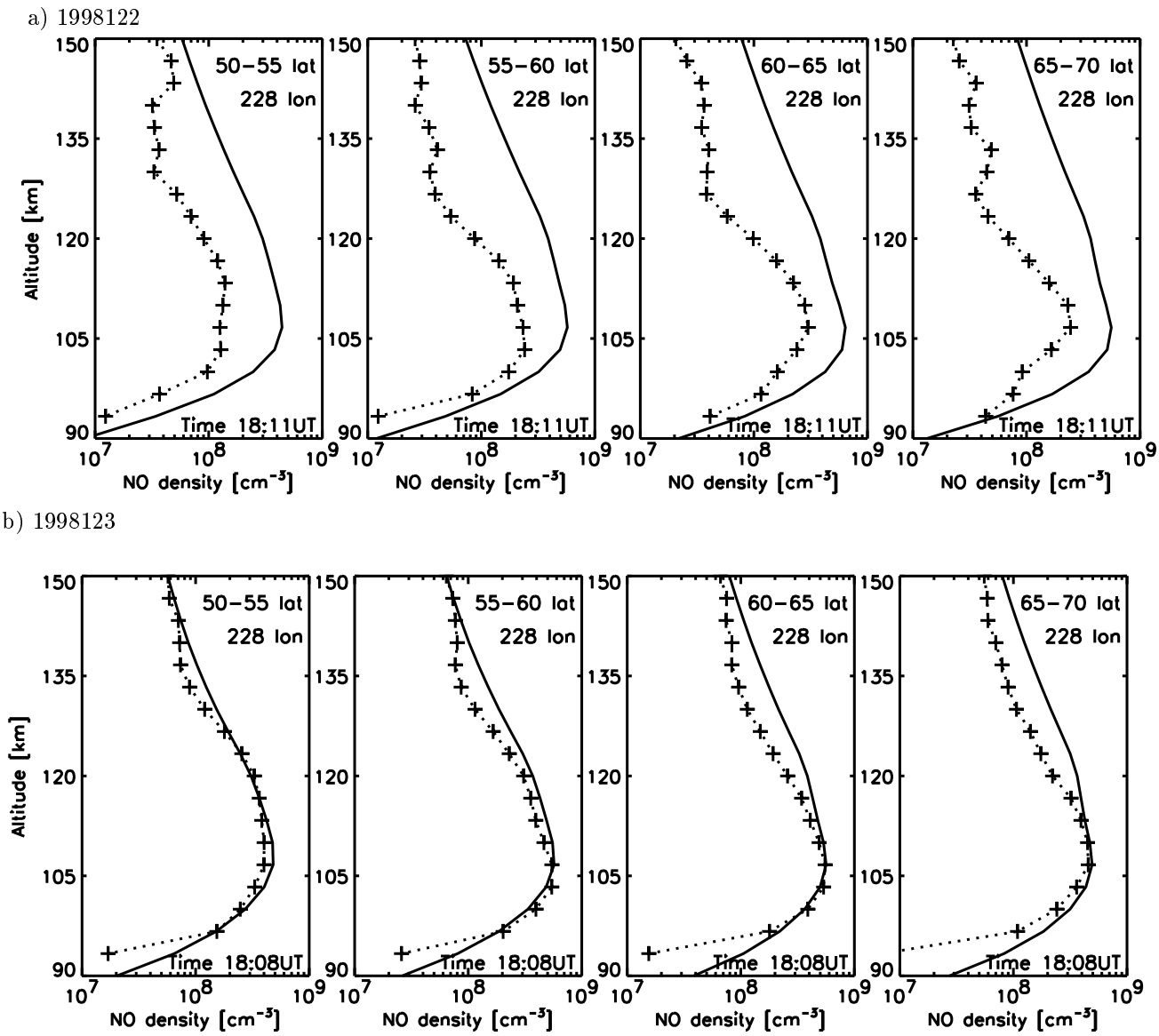

Figure 8. NO density at 228° east, four latitude regions, as measured by SNOE (dotted line with crosses) and calculated from the NOx model (solid line). The upper four plots are for day 122, and the lower four plots are the same regions for day 123. The universal time for the SNOE measurements at 60°N are given in the lower right corner of each plot.

The results from this study show that the photochemical model overestimates, to a varying degree, the nitric oxide density in the lower thermosphere during geomagnetic active periods. The work of *Siskind et al.* [1989a] was based on this same photochemical model, and had as input for the auroral energy deposition the hemispherical power index from the NOAA measurements, and a statistical model for the auroral precipitation pattern. Their model calculations gave a far greater NO density at higher latitudes than that measured by SME. Their differences were of a factor of four on the day before the geomagnetic storm, and a factor of ten after the storm. While they used a yield of 0.6 for the production of N(2D) from the electron impact on N2, we use a yield of 0.54 [*Zipf et al.*, 1980]. The calculated nitric oxide density is very sensitive to this branching ratio [Barth, 1992]. Changing from 0.60 to 0.54 produces a factor of two change in the nitric oxide density. From the UVI and PIXIE measurements we also get the structure and time history of the electron precipitation, without having to use a statistical model. Our results show a factor of 2-3 difference between model and SNOE measurements, for the day of the storm onset. This is a significant difference, however, quite better than a factor of 10 difference. The good correlation for the lower latitudes in the previous study by *Barth and Bailey* [2004], also indicates that the revised N(^{2}D) yield provides a more correct estimate of the nitric oxide production. The results of the present study, are substantially better for the day after the storm onset (123), when the atmosphere was calmer. This was also

the case for another event, not presented here, for days 176 to 178, 1998. The day of the geomagnetic storm, 177, the difference between the modeled and the measured NO density was more than a factor of 2. The next day, 178, the agreement between the model and the observations was remarkably good. This event was a rather isolated geomagnetic storm, and only the electron energy parameters derived from UVI and PIXIE observations during the event, were used as input to the NOx model, not a continuous energy flux as for the event presented here.

Sætre et al. [2006] compared the total energy deposition derived from SNOE nitric oxide measurements by use of the photochemical model, with that derived from PIXIE measurements for five geomagnetic events. Also for that study the model gave a lower auroral electron input from the SNOE measurements that derived from PIXIE.

The discrepancies between the modeled NO density and the measurements, might in part be due to the electron energy input to the model being wrong. Based on the good correlation on lower latitudes [*Barth and Bailey*, 2004], we believe that the method for the photoelectrons produced by solar soft X-rays and extreme ultraviolet, to be quite satisfactory also for the higher latitudes. Also for the results in this study, the modeled NO density agreed well with the observations when the auroral energy input was low. The auroral electron energy input for the model was mainly from UVI and PIXIE. For continuity of the energy input the electron energy flux was also derived from ground geomagnetic measurements from the SuperMAG database, in the time intervals without UVI and PIXIE measurements. The characteristic energy was for these cases set to a fixed value of 4 keV. The electron energy parameters were derived from the UVI and PIXIE measurements by using two different techniques, and then matched together to form one electron energy spectrum. We consider these results to be a satisfactory measure of the mean electron energy deposition into the lower thermosphere per hour. This hourly auroral energy input for the model was based on (usually) six energy spectra derived from UVI and PIXIE measurements. It is difficult to give an exact value for the uncertainty of this auroral energy flux and characteristic energy. There are no signs that they might be systematically overestimated, according to previous work where this method was used [*Østgaard et al.*, 2000].

The SuperMAG parametrization was divided in 24° longitude sectors. The linear relation between the energy flux derived from UVI and PIXIE measurements and the $\Delta N<0$ perturbation of the geomagnetic field, had a correlation of 0.75. There were longitude sectors where the number of magnetometer stations was quite low, especially in Siberia. The derived energy flux in these regions might be underestimated. This could be the reason for the differences in the model NO density and the measured one on the night between 122 and 123, universal time, and on the evening on day 123. Here the SNOE measurements of NO showed an increase, while the modeled density was decreasing. For the regions at hand, the main electron input was derived from magnetometer data, and the sectors had few stations.

The fixed electron characteristic energy at 4 keV for the SuperMAG parametrization could also cause some discrepancy. However, the altitude profiles of NO seem to be more governed by the vertical winds from temperature gradients. The height of the maximum NO density was not particularly different for the modeled and the measured profile. The characteristic energy of the auroral electrons, and hence the altitude of the maximum energy deposition, seemed to be well described by both the UVI and PIXIE measurements and the fixed 4 keV value for the SuperMAG events.

The nitric oxide densities from SNOE dayglow measurements had a total uncertainty of about 20% [*Barth and Bailey*, 2004]. When also considering the good results between the photochemical model calculations and the measured NO density at low latitudes where photoelectrons are the source of the electron impact reactions [Barth and Bailey, 2004], neither the SNOE NO measurements, nor the SNOE solar soft X-ray observations should give the large discrepancies at higher latitudes.

The differences between the model and the measurements were more dominant on day 122, than on day 123. This was especially evident in the altitude profiles of the NO density (figure 8). One of the main differences between these two days was the amount of Joule heating. On day 122 the overall Joule heating after the onset of the geomagnetic storm was larger than on day 123 . On day 122 the global Joule heating exceeded 300 GW for about 10 hours (values from the Assimilative Mapping of Ionospheric Electrodynamics (AMIE) procedure). This is considered to be a moderate amount of heating. On day 123 it was above 300 GW for only ∼4 hours in total. During periods of significant Joule heating, the atmosphere at auroral latitudes will expand, and give an increase of molecules relative to atoms in the lower thermosphere. Outside the auroral oval, air that has a lower concentration of molecules is transported downward [*Burns et al.*, 2006]. The antisunward neutral wind across the pole, due to ion-neutral coupling and the convection pattern, will blow the disturbed N_2 rich air from auroral regions to middle latitudes around local midnight. As these regions co-rotate with the Earth, the disturbance is eventually brought to the dawn sector. At mid-latitudes, there is a poleward return flow of the neutral winds, bringing air that has a lower N_2 mixing ratio to higher latitudes (around 130 km altitude). This N_2 poor air may then be located beneath regions of N_2 rich air [*Burns et al.*, 2006]. If this happens, the hydrostatic balance is broken for the lower thermospheric regions. The model for the background atmosphere used here, NRLMSISE-00, is based on the assumption that the atmosphere is in hydrostatic

equilibrium [*Bates*, 1959]. Hence, for periods when there is substantial Joule heating, the NRLMSISE-00 model will not be sufficient for modeling the correct response of the atmosphere. Instead, a global circulation model such as the NCAR TIME-GCM model, could be used to determine the background neutral atmosphere during disturbed conditions, and then the NOx one-dimensional model can be used for calculating the nitric oxide density. The heating on day 122 was considerable enough that the atmosphere was not in hydrostatic equilibrium this day, and the NO observations could therefore not be modeled correctly by the NOx model with the NRLMSISE-00 estimation for the background atmosphere. For the lower and middle latitudes the atmosphere was not affected to that extent by the amount of Joule and particle heating. The results for this study are hence not in conflict with the previous high correlation results for the tropics [*Barth and Bailey*, 2004]. The better correlations on day 123 show that when the atmosphere settles down and the effect of the Joule heating is not as dominant, the NOx model works much better. However, since the processes the day before were not fully covered by the model, the calculated increase often gave too high density for day 123 as well.

5. Summary and conclusion

The auroral electron energy has been derived from UVI and PIXIE measurements of auroral UV emissions and X-ray bremsstrahlung. For the times when the two instruments were not measuring the northern auroral oval, the electron energy was estimated from ground geomagnetic measurements. The auroral energy was arranged in geographical boxes of 5° latitude and 24° longitude sectors. It was continuous in time over four days, from day 120 until day 124 of 1998. This period covered the onset of a geomagnetic storm on the morning of day 122. The auroral energy was used as the input to a photochemical model for nitric oxide. The energy input from photoelectrons was also accounted for. The modeled NO density in the lower thermosphere between latitudes 50° and 70°N was compared with the NO density measured by SNOE for the same geographical area. Before the onset of the geomagnetic storm, the model seemed to work well when the auroral electron energy input was rather low. The results of this comparison showed an overestimation of the NO density by the photochemical model. This calculation is very sensitive to the branching ratio of electron impact dissociation of nitric oxide to produce $N(^2D)$ atoms. There also seemed to be better agreement between the model and measurements one day after the storm, even though the geomagnetic activity remained high. We believe the Joule heating effect on the background atmosphere was not properly captured by the NRLMSISE-00 model for the day of the storm, and that this led to the large overestimate of the NO density for that day. The day after, when the atmosphere was calmer, the difference between the modeled and measured NO densities was smaller. The reactions involved in the model, and their reaction rates and branching ratios, are probably sufficiently accurate to calculate the chemical production and loss of nitric oxide in the lower thermosphere. It is vital, though, to have the background atmosphere correctly portrayed. Some of the reactions are directly dependent on the neutral temperature of the atmosphere. All of the reactions need a correct description of the density of the neutral constituents.

To conclude, the photochemical model for NO, with NRLMSISE-00 as the model for the background atmosphere, is unable to calculate precisely the correct NO density in the lower thermosphere for periods with significant Joule heating. Based on the rather good agreement between the modeled nitric oxide density and the measurements before and after the geomagnetic storm, we believe that the chemical processes of the NOx model are a correct description of the nitric oxide production and loss in the auroral region.

Acknowledgments.

The Norwegian authors thank the Research Council of Norway for financial support.

For the ground magnetometer data we gratefully acknowledge: The S-RAMP Database, PI Prof. K. Yumoto and Dr. K. Shiokawa; The SPIDR database; Intermagnet; The institutes who maintain the IMAGE magnetometer array; AARI data, PI Prof. Oleg Troshichev; Danish Meteorological Institute, Mr. Ole Rasmussen and Project Scientist Dr. Jurgen Watermann; the CARISMA, PI Dr. Ian Mann; The MACCS program, PIs Dr. W. J. Hughes and Dr. M. Engebretson as well as the Geomagnetism Unit of the Geological Survey of Canada; GIMA, PI Prof. John Olson; MEASURE, UCLA IGPP and Florida Institute of Technology; USGS, Dr. Jeffrey J. Love; MAGIC, PI. Dr. C. Robert Clauer; SAMBA, PI Dr. Eftyhia Zesta; 210 Chain, PI K. Yumoto; SAMNET, PI Prof. Farideh Honary; IMAGE, PI Dr. Ari Viljanen.

We also thank Gang Lu for Joule heating data from the AMIE model.

References

Ahn, B. H., B. A. Emery, H. W. Kroehl, and Y. Kamide (1999), Climatological characteristics of the auroral ionosphere in terms of electric field and ionospheric conductance, *J. Geophys. Res.*, *104*, 10,031.

Bailey, S. M., T. N. Woods, C. A. Barth, S. C. Solomon, L. R. Canfield, and R. Korde (2000), Measurements of the solar soft x-ray irradiance by the Student Nitric Oxide Explorer: First analysis and underflight calibrations, *J. Geophys. Res.*, *105*, 27,179.

Bailey, S. M., C. A. Barth, and S. C. Solomon (2002), A model of nitric oxide in the lower thermosphere, *J. Geophys. Res.*, *107*, 1206.

Banks, P. M., and A. F. Nagy (1970), Concerning the influence of elastic scattering upon photoelectron transport and escape, *J. Geophys. Res.*, *75*, 1902.

Barth, C. (1992), Nitric oxide in the lower thermosphere, *Planet. Space Sci.*, *40*, 315.

Barth, C. A., and S. M. Bailey (2004), Comparison of a thermospheric photochemical model with Student Nitric Oxide Explorer (SNOE) observations of nitric oxide, *J. Geophys. Res.*, *109*(A03304), doi:10.1029/2003JA010227.

Barth, C. A., S. M. Bailey, and S. C. Solomon (1999), Solar-terrestrial coupling: Solar soft x-rays and thermospheric nitric oxide, *Geophys. Res. Lett.*, *26*, 1251.

Barth, C. A., D. N. Baker, and S. M. Bailey (2004), Seasonal variation of auroral electron precipitation, *Geophys. Res. Lett.*, *31*, doi:10.1029/2003GL018892.

Bates, D. R. (1959), Some problems concerning the terrestrial atmosphere above about the 100 km level, *Proc. R. Soc. London*, *253*(Ser. A), 451.

Baumjohann, W., and Y. Kamide (1984), Hemispherical Joule heating and the AE indices, *J. Geophys. Res.*, *89*, 383.

Burns, A. G., W. Wang, T. L. Killeen, S. C. Solomon, and M. Wiltberger (2006), Vertical variations in the N_2 mass mixing ratio during a thermospheric storm that have been simulated using a coupled magnetosphere-ionosphere-thermosphere model, *J. Geophys. Res.*, *111*(A11309), doi: 10.1029/2006JA011746.

Cleary, R. J. (1986), Daytime high-latitude rocket observations of the NO γ, δ and ε bands, *J. Geophys. Res.*, *91*, 11,337.

Foster, J. C., J. M. Holt, R. G. Musgrove, and D. S. Evans (1986), Ionospheric convection associated with discrete levels of particle precipitation, *Geophys. Res. Lett.*, *13*, 656.

Fuller-Rowell, T. J., and D. S. Evans (1987), Height-integrated Pedersen and Hall conductivity patterns inferred from the TIROS-NOAA satellite data, *J. Geophys. Res.*, *92*, 7606.

Germany, G. A., G. K. Parks, M. J. Brittnacher, J. Cumnock, D. Lummerzheim, J. F. Spann, L. Chen, P. G. Richards, and F. J. Rich (1997), Remote determination of auroral energy characteristics during substorm activity, *Geophys. Res. Lett.*, *24*, 995.

Germany, G. A., G. K. Parks, M. J. Brittnacher, J. F. Spann, J. Cumnock, D. Lummerzheim, F. J. Rich, and P. G. Richards (1998a), Energy characterization of a dynamic auroral event using GGS UVI images, in *Geospace Mass and Energy Flow: Results From the International Solar-Terrestrial Physic Program*, edited by J. L. Horwitz, D. L. Gallagher, and W. K. Peterson, Geophys. Monogr. Ser., p. 143, AGU, Washington, D. C.

Germany, G. A., J. F. Spann, G. K. Parks, M. J. Brittnacher, R. Elsen, L. Chen, D. Lummerzheim, and M. H. Rees (1998b), Auroral observations from the Polar Ultraviolet Imager (UVI), in *Geospace Mass and Energy Flow: Results From the International Solar-Terrestrial Physic Program*, edited by J. L. Horwitz, D. L. Gallagher, and W. K. Peterson, Geophys. Monogr. Ser., p. 149, AGU, Washington, D. C.

Gjerloev, J. W., and R. A. Hoffmann (2001), The convection electric field in auroral substorms, *J. Geophys. Res.*, *106*, 12,919.

Gjerloev, J. W., M. Friel, R. A. Hoffman, K. Takahashi, R. Barnes, C. Meng, and R. A. Greenwald (2004), The global magnetometer network initiative: SuperMAG, *Eos Trans. AGU, 85(47), Fall Meet. Suppl., Abstract SH41A-1079.*

Hinteregger, H. E., K. Fukui, and B. R. Gilson (1981), Observational, reference, and model data on solar EUV, from measurements on AE-E, *Geophys. Res. Lett.*, *8*, 1147.

Imhof, W. L., et al. (1995), The Polar Ionospheric X-ray Imaging Experiment (PIXIE), *Space Sci. Rev.*, *71*, 385.

Kamide, Y., and S. Kokubun (1996), Two-component auroral electrojet: Importance for substorm studies, *J. Geophys. Res.*, *101*, 13,027.

Kamide, Y., and J. F. Vickrey (1983), Relative contribution of ionospheric conductivity and electric field to the auroral electrojets, *J. Geophys. Res.*, *88*, 7989.

Minschwaner, K., and D. E. Siskind (1993), A new calculation of nitric oxide photolysis in the stratosphere, mesosphere, and lower thermosphere, *J. Geophys. Res.*, *98*, 20,401.

Østgaard, N., J. Bjordal, J. Stadsnes, and E. Thorsen (1999), PIXIE data processing at the University of Bergen. Tecnical report, *Tech. Rep. 1999-05*, Dept. of Physics, University of Bergen, Bergen, Norway.

Østgaard, N., J. Stadsnes, J. Bjordal, R. R. Vondrak, S. A. Cummer, D. L. Chenette, M. Schulz, and J. G. Pronko (2000), Cause of the localized maximum of x-ray emission in the morning sector: A comparison with electron measurements, *J. Geophys. Res.*, *105*, 20,869.

Østgaard, N., J. Stadsnes, J. Bjordal, G. A. Germany, R. R. Vondrak, G. K. Parks, S. A. Cummer, D. L. Chenette, and J. G. Pronko (2001), Auroral electron distributions derived from combined UV and X-ray emissions, *J. Geophys. Res.*, *106*, 26,081.

Østgaard, N., R. R. Vondrak, J. W. Gjerloev, and G. Germany (2002), A relation between the energy deposition by electron precipitation and geomagnetic indices during substorms, *J. Geophys. Res.*, *107*(A9), 1246, doi:10.1029/2001JA002003.

Picone, J. M., A. E. Hedin, D. P. Drob, and A. C. Aikin (2002), NRLMSISE-00 empirical model of the atmosphere: Statistical comparisons and scientific issues, *J. Geophys. Res.*, *107*, doi:10.1029/2002JA009430.

Randall, C. E., V. L. Harvey, C. S. Singleton, P. F. Bernath, C. D. Boone, and J. U. Kozyra (2006), Enhanced NO_x in 2006 linked to strong upper stratospheric Arctic vortex, *Geophys. Res. Lett.*, *33*, doi:10.1029/2006GL027160.

Randall, C. E., et al. (2005), Stratospheric effects of energetic particle precipitation in 2003-2004, *Geophys. Res. Lett.*, *32*, doi:10.1029/2004GL022003.

Sætre, C., C. A. Barth, J. Stadsnes, N. Østgaard, S. M. Bailey, D. N. Baker, and J. W. Gjerloev (2006), Comparisons of electron energy deposition derived from observations of lower thermospheric nitric oxide and from X-ray bremsstrahlung measurements, *J. Geophys. Res.*, *111*, doi:10.1029/2005JA011391.

Siskind, D. E., C. A. Barth, D. S. Evans, and R. G. Roble (1989a), The response of thermospheric nitric oxide to an auroral storm: 2. Auroral latitudes, *J. Geophys. Res.*, *94*, 16,899.

Siskind, D. E., C. A. Barth, and R. G. Roble (1989b), The response of thermospheric nitric oxide to an auroral storm: 1. Low and middle latitudes, *J. Geophys. Res.*, *94*, 16,885.

Siskind, D. E., C. A. Barth, and D. D. Cleary (1990), The possible effect of solar soft X rays on thermospheric nitric oxide, *J. Geophys. Res.*, *95*, 4311.

Siskind, D. E., D. J. Strickland, R. R. Meier, T. Majeed, and F. G. Eparvier (1995), On the relationship between the solar soft X-ray flux and thermospheric nitric oxide: An update with an improved photoelectron model, *J. Geophys. Res.*, *100*, 19,687.

Solomon, S., P. J. Crutzen, and R. G. Roble (1982), Photochemical coupling between the thermosphere and the lower atmosphere, 1, Odd nitrogen from 50 to 120 km, *J. Geophys. Res.*, *87*, 7206.

Solomon, S. C., and V. J. Abreu (1989), The 630-nm dayglow, *J. Geophys. Res.*, *94*, 6817.

Solomon, S. C., P. B. Hays, and V. J. Abreu (1988), The auroral 6300 å emission: Observations and modeling, *J. Geophys. Res.*, *93*, 9867.

Solomon, S. C., S. M. Bailey, and T. N. Woods (2001), Effect of solar soft X-rays on the lower ionosphere, *Geophys. Res. Lett.*, *28*, 2149.

Sugino, M., R. Fujii, S. Nozawa, S. C. Buchert, H. J. Opgenoorth, and A. Brekke (2002), Relative contribution of ionospheric conductivity and electric field to ionospheric current, *J. Geophys. Res.*, *107*(A10), 1330.

Torr, M. R., et al. (1995), A far ultraviolet imager for the International Solar-Terrestrial physics mission, *Space Sci. Rev.*, *71*, 329.

Zipf, E. C., P. J. Epsy, and C. F. Boyle (1980), The exciattion and collisional deactivation of metastable $N(^2P)$ atoms in auroras, *J. Geophys. Res.*, *85*, 687.

C. Sætre, J. Stadsnes, N. Østgaard Department of Physics and Technology, University of Bergen, N-5007 Bergen, Norway. (camilla.satre@ift.uib.no)

C. A. Barth, D. N. Baker, Laboratory for Atmospheric and Space Physics, University of Colorado, Boulder, CO 80303-7814, USA.

S. M. Bailey, Geophysical Institute, University of Alaska, Fairbanks, AK 99775-7320, USA.

J. W. Gjerloev, Applied Physics Laboratory, Johns Hopkins University, Laurel, MD 20723-6099, USA.

G. A. Germany, Center for Space Plasma and Aeronomic Research, University of Alabama in Huntsville, Huntsville, Alabama, USA

(Received _____)